Science Bulletin 71 (2026) 2977–2981

Contents lists available at ScienceDirect

Science Bulletin

journal homepage: www.elsevier.com/locate/scib

Short Communication

Large-scale distortion of the dayside magnetopause under radial interplanetary magnetic field

Jin Guo [a], San Lu [a,*], Quanming Lu [a,*], Boyi Wang [b], Shimou Wang [a], Junyi Ren [a], Jiuqi Ma [a], Xinliang Gao [a], Rajkumar Hajra [a], Rongsheng Wang [a]

[a] National Key Laboratory of Deep Space Exploration/School of Earth and Space Sciences, University of Science and Technology of China, Hefei 230026, China
[b] School of Aerospace Science, Harbin Institute of Technology (Shenzhen), Shenzhen 518055, China

ARTICLE INFO

Article history:
Received 24 September 2025
Received in revised form 7 January 2026
Accepted 8 January 2026
Available online 19 January 2026

The solar wind, a continuous stream of charged particles emitted from the Sun's upper atmosphere, exerts a profound influence on celestial bodies throughout the solar system [1]. For planets with intrinsic magnetic fields, such as Earth, this particle stream interacts with the planetary magnetic field, forming a protective bubble known as the magnetosphere [2]. The magnetopause, the outer boundary of the magnetosphere, serves as a protective shield against atmospheric erosion by limiting direct solar-wind penetration and regulating energy transfer from the solar wind into the magnetosphere [2,3].

Magnetic reconnection, which occurs when the interplanetary magnetic field (IMF) is oriented opposite to the geomagnetic field, mediates the morphology and dynamics of the magnetopause [3]. Under southward IMF conditions, low-latitude reconnection drives dayside magnetospheric erosion and nightside replenishment, compressing the dayside magnetopause while expanding its nightside counterpart [4]. Conversely, northward IMF orientations favor high-latitude lobe reconnection, reversing this dayside-nightside asymmetry [4,5].

Although southward and northward IMF scenarios have been extensively characterized, the magnetopause response to radial IMF configurations (i.e., when the IMF aligns with the solar-wind flow direction) remains poorly understood, constituting a critical knowledge gap in space plasma physics. Radial IMF conditions are particularly favorable for generating magnetosheath high-speed jets [6], which are localized plasma structures whose dynamic pressures exceed ambient values [7]. These jets can induce magnetopause indentations [8,9] and trigger intermittent magnetic reconnection [10]. However, conventional wisdom suggests that such perturbations remain spatially confined (typically several Earth radii) [8,9], limiting their ability to mediate substantial solar-wind energy transfer into the magnetosphere. In this study, using serendipitous joint observations from spacecraft and ground stations, together with a global hybrid simulation, we report a large-scale distortion of the dayside magnetopause that manifests as coexisting sunward-protruding bulges and cusp-to-cusp valleys during a prolonged radial IMF interval (>30 min).

During the event on 12 August 2007 (~14:30 UT), the four Time History of Events and Macroscale Interactions during Substorms (THEMIS, Text S1 online) spacecraft were positioned in a string-of-pearls configuration near the subsolar magnetopause and in the adjacent magnetosheath. Concurrently, the solar-wind conditions were measured by the Advanced Composition Explorer (ACE, Text S1 online) spacecraft at the L1 Lagrange point (~220 R_E upstream). The IMF cone angle ranged from 3.3° and 6.2°, and B_y and B_z components constituted only 7% and 10% of $|B|$, respectively, confirming a predominantly radial IMF orientation (Fig. S1 online). No solar-wind dynamic pressure pulses or discontinuities were detected. This case was previously reported by Shue et al. [11].

Here we demonstrate a previously unrecognized large-scale distortion of the dayside magnetopause using coordinated observations from the Automatic Geophysical Observatory (AGO, Text S2 online) and the THEMIS spacecraft (Fig. 1). At ~14:33:15 UT (Fig. 2a), THA was situated in the magnetosheath (Fig. 1a) and detected a magnetosheath jet (Jet 1) lasting ~103 s, with an earthward flow (Fig. 1b) and a peak dynamic pressure of ~1.8 nPa (Fig. 1c, red-shaded interval). The peak dynamic pressure exceeded 0.5 times the solar-wind dynamic pressure (~1.2 nPa), confirming the presence of a magnetosheath jet [7]. Concurrently, THB was positioned within the magnetosphere (Fig. 1d), and THC was traversing the magnetopause (Fig. 1g). When THC crossed the mag-

* Corresponding authors.
E-mail addresses: lusan@ustc.edu.cn (S. Lu), qmlu@ustc.edu.cn (Q. Lu).

https://doi.org/10.1016/j.scib.2026.01.032
2095-9273/

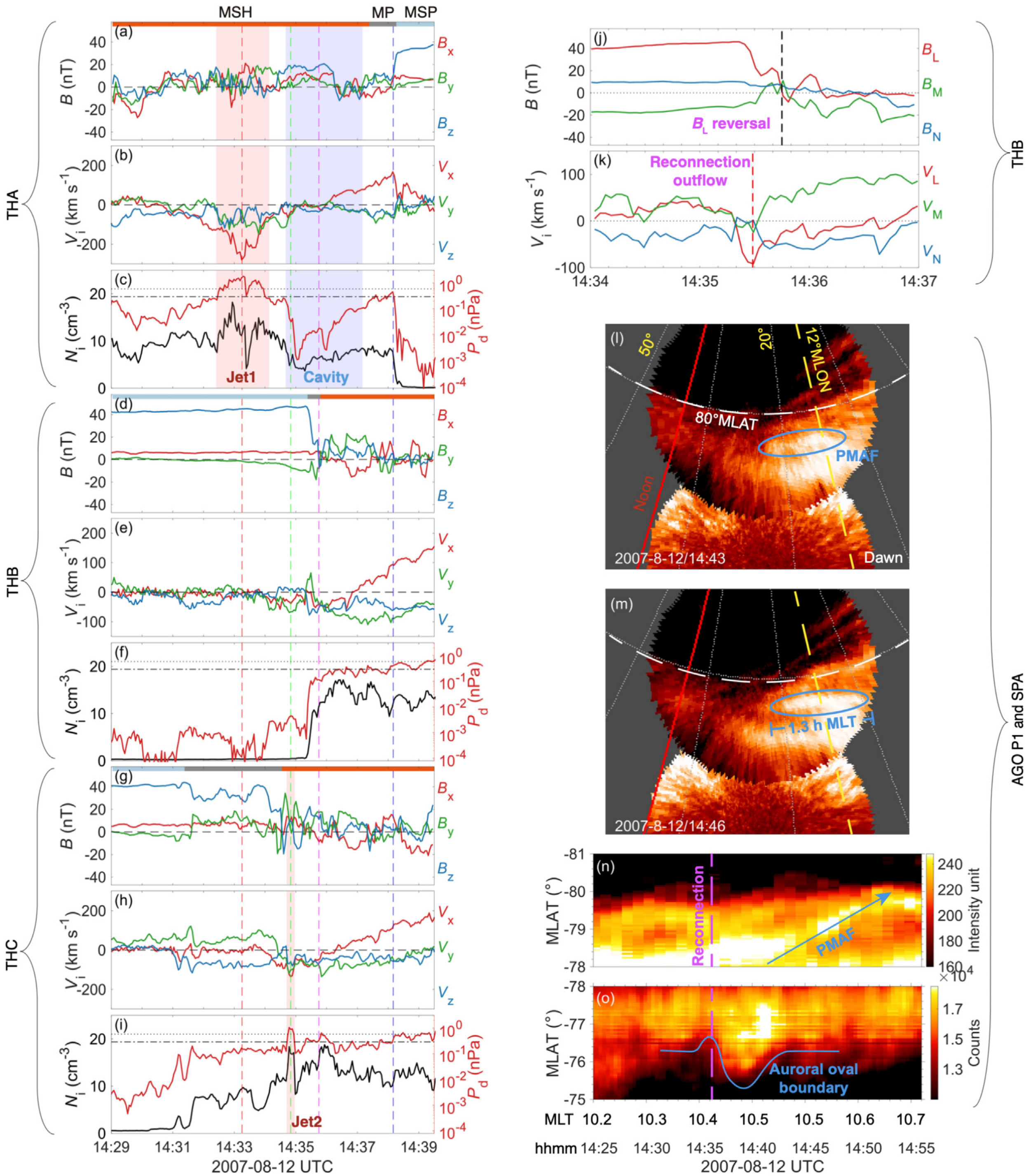

Fig. 1. Spacecraft and ground-based observations of large-scale magnetopause distortion. (a–i) THA, THB, and THC measurements in the magnetosheath from 14:29:00 UT to 14:39:30 UT on 12 August 2007. (a, d, g) GSM magnetic-field components. (b, e, h) GSM ion-velocity components. (c, f, i) Ion density and dynamic pressure. The red- and blue-shaded interval denote magnetosheath jets and magnetosheath cavity, respectively. Time intervals when the spacecraft were in the magnetosheath (MSH), magnetopause (MP), and magnetosphere (MSP) are marked by red, grey, and blue bars at the top of panels (a), (d), and (g), respectively. These intervals were identified primarily using the electron differential energy flux (Fig. S2 online), supplemented by magnetic-field, ion-velocity, and density measurements. Because THC and THD were in close proximity (~0.1 R_E) and show nearly identical observations (Fig. S3 online), only THC data are presented. At the time of interest, THA, THB, and THC were located at 11.76, 11.94, and 11.90 MLT, respectively. THE is not considered due to missing data. (j–k) THB observations of magnetopause reconnection associated with a magnetosheath jet from 14:24 UT to 14:37 UT on 12 August 2007. (j) Magnetic-field components in LMN coordinates. (k) Ion-velocity components in LMN coordinates. The red dashed line marks the reconnection outflow, and the black dashed line marks the B_L reversal during reconnection. (l–o) AGO P1 and SPA optical observations of PMAFs associated with magnetopause reconnection. (l, m) Snapshots of 630.0-nm emission observed at AGO P1 (14:43:00 UT) and SPA (14:46:00 UT) on 12 August 2007. The red line indicates 12 MLT; the left and right sides correspond to the post-noon and pre-noon sectors, respectively. The 630.0–nm emission is used as an auroral indicator because it is particularly sensitive to soft (low–energy) electron precipitation and is commonly used to identify PMAFs and other cusp activity [13] (Fig. S5 online). (n, o) Keograms of 630.0-nm emission at AGO P1 and SPA along ~12° MLON (yellow dashed lines in panels l and m), respectively.

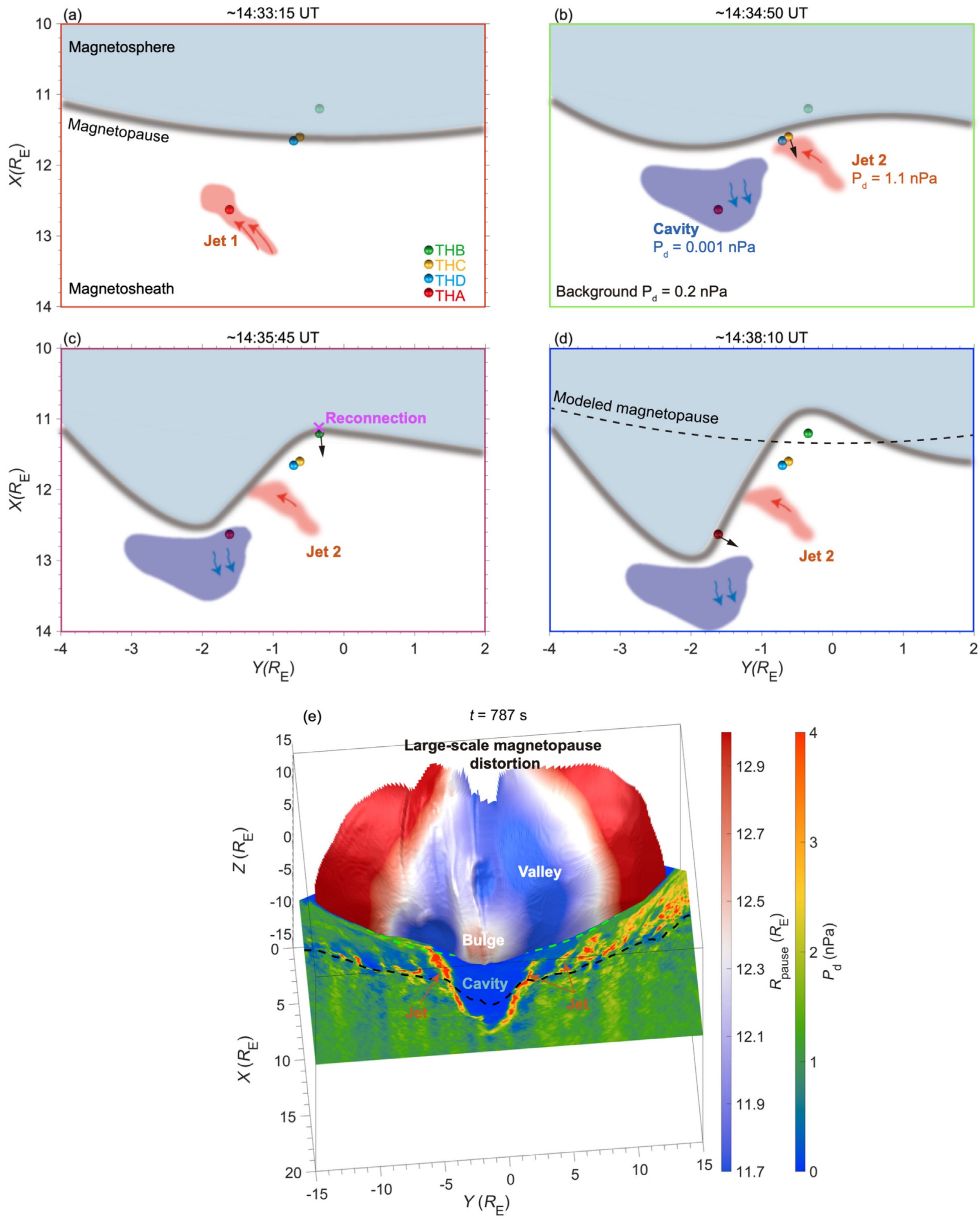

Fig. 2. Magnetopause distortion reconstructed from observations and a three-dimensional global hybrid simulation. (a–d) Large-scale magnetopause distortion and reconnection caused by a magnetosheath cavity and jet observed by THEMIS in the plane $z = -3.2R_E$. The magnetopause is shown by gray solid curves, and the black arrows indicate the magnetopause normal direction. (a) At ~14:33:15 UT, THA observed a magnetosheath jet; THC and THD were crossing the magnetopause; THB was in the magnetosphere. (b) At ~14:34:50 UT, THA observed a magnetosheath cavity with low dynamic pressure (~0.001 nPa); THC and THD observed another jet with high dynamic pressure (~1.1 nPa); THB remained in the magnetosphere. The background magnetosheath dynamic pressure is ~0.2 nPa. (c) At ~14:35:45 UT, THA was still inside the cavity; THC and THD were in the magnetosheath; THB crossed the magnetopause and observed reconnection. (d) At ~14:38:10 UT, THA crossed the magnetopause; THC, THD, and THB were in the magnetosheath. The dashed curve indicates the magnetopause predicted by the magnetopause model. (e) Dynamic pressure, P_d, in the plane $z = 1.5R_E$ and the distance from Earth's center to the magnetopause, R_{pause}. The shown 3-D surface represents the magnetopause identified from magnetic-field-line topology (Fig. S8 online). The green dashed curve indicates the magnetopause predicted by the magnetopause model, and the black dashed curve indicates the bow shock. The simulated magnetopause distortion in the y-direction exceeds the observational estimate, possibly because the maximum spacecraft separation was only ~1.3 R_E, making the observational value a conservative lower bound.

netopause (~14:34:13 UT), the magnetopause normal direction was (0.973, 0.148, 0.180), deviating by only 6° from the magnetopause model prediction [12] (Table S1 online), indicating no significant distortion at this time.

At ~14:34:50 UT (Fig. 2b), THA detected a magnetosheath cavity characterized by low dynamic pressure (~0.001 nPa, Fig. 1c). Concurrently, THB remained within the magnetosphere (Fig. 1d). THC, however, had entered the magnetosheath and detected another magnetosheath jet (Jet 2, Fig. 1h and i). This jet persisted for ~16 s and exhibited a peak dynamic pressure of ~1.1 nPa. The ambient dynamic pressure in the magnetosheath was ~0.2 nPa. Fig. 2b illustrates the spatial configuration of the cavity, jets, and the magnetopause, together with the magnetopause normal direction (black arrow). Given that the dynamic pressure in the cavity and jet regions was ~0.005 and ~5.5 times the background magnetosheath value, respectively, significant distortion of the magnetopause was anticipated.

At ~14:35:45 UT (Fig. 2c), THA remained within the cavity (Fig. 1c), while THC was situated in the magnetosheath (Fig. 1g). Concurrently, THB was crossing the magnetopause (Fig. 1d), and the normal direction was measured as (0.992, 0.095, 0.084), deviating by 18° from the magnetopause model prediction. This suggests that the jet and cavity altered the magnetopause, forming an indentation. During THB's passage through the magnetopause, the magnetic-field components B_y and B_z reversed (Fig. 1d), and the velocity components $V_{i,y}$ and $V_{i,z}$ peaked (Fig. 1e), indicating magnetopause reconnection. To examine the reconnection signatures more effectively, the data are presented in a current-sheet *LMN* coordinate system, where **N =** (0.992, 0.095, 0.084) represents the current-sheet normal direction, **L =** (−0.028, −0.475, 0.880) is aligned with the antiparallel magnetic-field direction, and **M = N** × **L =** (0.124, −0.875, −0.468) follows the current direction in GSM coordinates. The *L* component of the magnetic field, B_L, reversed at 14:35:45 UT (black dashed line, Fig. 1j) when THB traversed the reconnection outflow region. The reconnection outflow in the *L* direction, $V_{i,L}$, intensified at 14:35:29 UT (red dashed line, Fig. 1k). Because magnetopause reconnection is asymmetric, the peak in $V_{i,L}$ does not coincide with the B_L reversal: the outflow jet peaks closer to the magnetosphere side, whereas the B_L reversal occurs nearer the magnetosheath side (Fig. S4 online). The reconnection outflow region's extent in the *N* direction, determined by integrating the *N* component of plasma velocity V_N from 14:35:18 UT to 14:35:49 UT, is ~1147 km, equivalent to ~18 ion inertial lengths. Additionally, a Walén test corroborates that THB observed a reconnection outflow (Text S3 online). Here $\Delta\boldsymbol{V}_{\rm obs}$ denotes the velocity change across the magnetopause observed by the spacecraft. In the THEMIS observations, the observed and predicted outflow velocity changes ($\Delta\boldsymbol{V}_{\rm obs}$ and $\Delta\boldsymbol{V}_{\rm pre}$) differed by 3% in magnitude and 32° in direction, yielding $\Delta V^* = 0.87$, much larger than 0.5, indicating that THB observed a reconnection outflow.

Auroral observations at the AGO P1 and South Pole A (SPA) stations provide additional evidence for magnetopause reconnection. After 14:35:00 UT, a poleward moving auroral form (PMAF; an ionospheric signature of magnetopause reconnection and flux transfer [13]) formed over the Antarctic ionosphere (Fig. 1l–o). At 14:46:00 UT, the PMAF was located in the pre-noon sector, spanning ~9.9–11.2 h magnetic local time (MLT) (Fig. 1m) and was nearly co-located with the inferred footprint of the magnetopause reconnection site at ~11.9 h MLT observed by THB. The remaining offset may result from dawnward migration of the magnetopause reconnection site [14]. Based on the PMAF's dawn-dusk extent, the spatial extent of reconnection X-line in the dawn-dusk direction is estimated to be ~4 $R_{\rm E}$[15]. After 14:35:00 UT, the auroral oval boundary at 12° magnetic longitude (MLON), known as the open-close field-line boundary [16], extended equatorward from −77° to −75.8° magnetic latitude (MLAT), as shown in Fig. 1o. According to the TS05 magnetic field model [17], this variation in magnetic latitude at the auroral oval boundary corresponds to a magnetopause displacement of ~0.5 $R_{\rm E}$ in the *x*-direction near the subsolar point, indicating that the magnetosphere's magnetic flux was eroded by magnetopause reconnection.

Around 14:38:10 UT (Fig. 2d), THA crossed the magnetopause (Fig. 1a), and the magnetopause normal direction was (0.640, 0.742, −0.201), deviating by 54° from the direction predicted by the magnetopause model. Concurrently, THB and THC were situated in the magnetosheath (Fig. 1d and g), indicating significant distortion of the magnetopause with deflections of at least ~1.5 $R_{\rm E}$ in the *x*-direction and ~1.3 $R_{\rm E}$ in the *y*-direction (Fig. 2d).

These conjugate observations reveal a coherent mechanism for dayside magnetopause distortion. Under a radial IMF, a magnetosheath jet impinges on and dents the magnetopause (Fig. 2c), initiating reconnection (Fig. 1j and k) and flux transfer. The corresponding PMAF, recorded by AGO (Fig. 1l–n), indicates that the reconnection X-line extends ~4 $R_{\rm E}$ in the dawn–dusk (GSM *y*) direction. Magnetopause reconnection erodes the dayside magnetosphere from the equator toward the cusps over a dawn–dusk extent of several $R_{\rm E}$. The equatorward motion of the noon-sector auroral oval boundary (Fig. 1o) provides evidence of magnetospheric erosion and indicates the formation of a magnetopause valley. Concurrently, the reduced dynamic pressure inside the magnetosheath cavity (Fig. 1c) drives a sunward bulge adjacent to the valley (Fig. 2c). The bulge and the valley constitute a pronounced large-scale distortion of the dayside magnetopause.

While detailed spacecraft data analysis provides key insights into the large-scale distortion of the dayside magnetopause, further support for the observation-based interpretation and a broader picture of the process comes from a 3-D global hybrid computer simulation. Fig. 2e presents the global picture of the magnetopause distortion from such a simulation, in which solar-wind parameters observed by spacecraft at the L1 point were used as inputs (see Text S4 online for further details of the simulation parameters). Because the solar wind is super-Alfvénic, a bow shock forms outside the magnetosphere (indicated by the black dashed curve). By comparing the magnetopause position from the simulation with the magnetopause model [12], it is evident that near the subsolar point the magnetopause experiences significant distortion, measuring ~1.4 $R_{\rm E}$ in the *x*-direction and ~5 $R_{\rm E}$ in the *y*-direction from the bulge to the valleys (Fig. 2e). Numerous magnetosheath jets impinge on the magnetopause, and these jets trigger multi-site magnetic reconnection, sustaining continuous erosion of the magnetosphere over an extended period and ultimately producing large-scale magnetopause valleys (Figs. S6 and S7 online).

Our study, combining serendipitous multi-point spacecraft observations, ground-based measurements, and a 3-D global hybrid simulation, reveals a previously unrecognized phenomenon: a large-scale distortion of Earth's dayside magnetopause under prolonged radial IMF conditions. This large-scale dayside distortion manifests as coexisting sunward-protruding bulges and cusp-to-cusp valley. The bulge is driven by a magnetosheath cavity with low dynamic pressure (~0.001 nPa, ~0.5% of the ambient value in the magnetosheath). The valleys, originating from localized indentations, span from the northern to southern polar regions and shift the magnetopause inward by about one Earth radius. The mechanism hinges on numerous magnetosheath jets continuously eroding the dayside magnetosphere via magnetic reconnection and flux transport, ultimately producing the valleys.

The occurrence of magnetopause valleys underscores the importance of sustained radial IMF intervals that enable cumulative reconnection, allowing numerous magnetosheath jets to act as persistent drivers of magnetospheric erosion. This finding challenges the conventional view that mesoscale magnetosheath jets primarily induce localized perturbations [6,8,9]; instead, it demonstrates their capacity to drive large-scale magnetospheric reconfiguration and enhanced solar wind-magnetosphere-ionosphere coupling. Jet driven reconnection at multiple sites, followed by flux transfer events, provides pathways for solar wind energy and plasma to enter the magnetosphere, with potential space-weather consequences.

Conflict of interest

The authors declare that they have no conflict of interest.

Acknowledgments

This work was supported by the National Key Research and Development Program of China (2025YFF0512100), the National Natural Science Foundation of China (42274196, 42174181, and 42508011), the Strategic Priority Research Program of Chinese Academy of Sciences (XDB0560000), the Fundamental Research Funds for the Central Universities (WK2080250226), and the China Postdoctoral Science Foundation (GZB20250097 and 2025M770380). Computer resources were provided by the Hefei Advanced Computing Center of China.

Author contributions

Jin Guo and San Lu analyzed the spacecraft data, performed the hybrid simulations, analyzed the simulation data, and wrote the manuscript. Quanming Lu conceived the idea and oversaw the project. Boyi Wang carried out the auroral observation analysis. Shimou Wang, Junyi Ren, Jiuqi Ma, Xinliang Gao, Rajkumar Hajra, and Rongsheng Wang contributed to the interpretation of the observation and simulation results. All of the authors made significant contributions to this work.

Data availability

THEMIS data are available at http://themis.ssl.berkeley.edu. ACE data are available at https://cdaweb.gsfc.nasa.gov/ or https://izw1.caltech.edu/ACE/. The simulation data can be downloaded from https://doi.org/10.57760/sciencedb.space.01877. The THEMIS data and ACE data were collected with the SPEDAS software (Space Physics Environment Data Analysis Software, http://spedas.org/blog) and analyzed by the IRFU package (https://github.com/irfu). The optical imaging data at AGO P1 and SPA station can be accessed online (http://sprg.ssl.berkeley.edu/atmos/ago_data.html). The global hybrid simulation code is available from https://doi.org/10.57760/sciencedb.space.02474.

Appendix A. Supplementary material

Supplementary data to this article can be found online at https://doi.org/10.1016/j.scib.2026.01.032.

References

[1] Kivelson MG, Russell CT. Introduction to space physics. Cambridge: Cambridge University Press; 1995.
[2] Russell CT. The dynamics of planetary magnetospheres. Planet Space Sci 2001;49:1005–30.
[3] Dungey JW. Interplanetary magnetic field and the auroral zones. Phys Rev Lett 1961;6:47–8.
[4] Lu S, Guo J, Lu QM, et al. Three-dimensional global hybrid simulations of plasma transport and energy conversion during solar wind-magnetosphere interactions. Geophys Res Lett 2025;52:e2025GL117084.
[5] Zhang QH, Zhang YL, Wang C, et al. A space hurricane over the Earth's polar ionosphere. Nat Commun 2021;12:1207.
[6] Plaschke F, Hietala H, Archer M, et al. Jets downstream of collisionless shocks. Space Sci Rev 2018;214:1–77.
[7] Hietala H, Laitinen TV, Andréeová K, et al. Supermagnetosonic jets behind a collisionless quasiparallel shock. Phys Rev Lett 2009;103:245001.
[8] Němeček Z, Šafránková J, Grygorov K, et al. Extremely distant magnetopause locations caused by magnetosheath jets. Geophys Res Lett 2023;50:e2023GL106131.
[9] Wang X, Lu JY, Wang M, et al. Simultaneous observation of magnetopause expansion under radial IMF and indention by HSJ. Geophys Res Lett 2023;50:e2023GL105270.
[10] Hietala H, Phan T, Angelopoulos V, et al. *In situ* observations of a magnetosheath high-speed jet triggering magnetopause reconnection. Geophys Res Lett 2018;45:1732–40.
[11] Shue JH, Chao JK, Song P, et al. Anomalous magnetosheath flows and distorted subsolar magnetopause for radial interplanetary magnetic fields. Geophys Res Lett 2009;36:L18112.
[12] Shue JH, Song P, Russell CT, et al. Magnetopause location under extreme solar wind conditions. J Geophys Res Space Phys 1998;103:17691–700.
[13] Sandholt PE, Farrugia CJ. Poleward moving auroral forms (PMAFs) revisited: responses of aurorae, plasma convection and Birkeland currents in the pre- and postnoon sectors under positive and negative IMF by conditions. Ann Geophys 2007;25:1629–52.
[14] Guo J, Wang BY, Lu S, et al. Azimuthal motion of poleward moving auroral forms. Geophys Res Lett 2022;49:e2022GL099753.
[15] Hwang KJ, Nishimura Y, Coster A, et al. Sequential observations of flux transfer events, poleward-moving auroral forms, and polar cap patches. J Geophys Res Space Phys 2020;125:e2019JA027674.
[16] Lorentzen DA, Deehr CS, Minow JI, et al. SCIFER-Dayside auroral signatures of magnetospheric energetic electrons. Geophys Res Lett 1996;23:1885–8.
[17] Tsyganenko NA, Sitnov MI. Modeling the dynamics of the inner magnetosphere during strong geomagnetic storms. J Geophys Res Space Phys 2005;110:A03208.